Cassini in Titan's tail: CAPS observations of plasma escape

A. J. Coates,[1,2] A. Wellbrock,[1,2] G. R. Lewis,[1,2] C. S. Arridge,[1,2] F. J. Crary,[3] D. T. Young,[3] M. F. Thomsen,[4] D. B. Reisenfeld,[5] E. C. Sittler Jr.,[6] R. E. Johnson,[7] K. Szego,[8] Z. Bebesi,[8] and G. H. Jones[1,2]

Received 3 February 2012; revised 28 March 2012; accepted 3 April 2012; published 23 May 2012.

[1] We present observations of CAPS electron and ion spectra during Titan distant tail crossings at 5,000–10,000 km altitude by the Cassini spacecraft. In common with closer tail encounters, we identify ionospheric plasma in the tail. Some of the electron spectra indicate a direct magnetic connection to Titan's dayside ionosphere due to the presence of ionospheric photoelectrons. Ion observations reveal heavy (m/q$\sim$ 16 and 28) and light (m/q = 1–2) ion populations streaming into the tail. Using the distant tail encounters T9, T75 and T63, we estimate total plasma loss rates from Titan via this process of (4.2, 0.96 and 2.3) $\times$ 10^{24} ions s^{-1} respectively for the three encounters, values which are in agreement with some simulations but slightly lower than earlier estimates based on non-differential techniques. Using the mass-separated data, this corresponds to mass loss rates of (8.9, 1.6, 4.0) $\times$ 10^{25} amu s^{-1} for T9, T75 and T63 respectively, an average loss rate of $\sim$7 tonnes per Earth day. Remarkably, all of the tail encounters studied here indicate a split tail feature, indicating that this may be a common feature in Titan's interaction with Saturn's magnetosphere.

Citation: Coates, A. J., et al. (2012), Cassini in Titan's tail: CAPS observations of plasma escape, *J. Geophys. Res.*, *117*, A05324, doi:10.1029/2012JA017595.

1. Introduction

[2] Cassini has revealed many important aspects of Titan's ionosphere (e.g., reviews by *Cravens et al.* [2009] and *Coates et al.* [2011a]). Titan, orbiting at 20 Saturn radii (R_s) from Saturn, spends most of its time in Saturn's magnetosphere, and recent papers have documented the variety of upstream conditions at Titan's orbit [*Rymer et al.*, 2009 *Arridge et al.*, 2011a]. A small percentage (<5%) of encounters indicate magnetosheath (shocked solar wind plasma outside the magnetopause) conditions upstream or very close by (e.g., *Bertucci et al.* [2008] for T32 and *Wei et al.* [2011] for T42).

[3] While in the magnetosphere, even at $20R_S$, the flow is still dominated by corotation. The associated electric field direction would be anti-Saturnward, if we can assume nominal encounter conditions, i.e., precise corotation and a North–South orientation of Saturn's magnetic field [e.g., *Blanc et al.*, 2002]. This, however, is not the case in general, e.g., the flow speed is usually less than the corotation speed, and during some flybys the magnetic field is dominated by its radial component. The exact orientation of the associated electric field, which orients the initial trajectories of pickup ions from Titan, varies significantly from encounter to encounter [*Simon et al.*, 2010; *Arridge et al.*, 2011a, 2011b; *Szego et al.*, 2011]. Clearly, the upstream plasma and field conditions play an important role in plasma escape from Titan.

[4] Before the Cassini mission, it had been anticipated that pickup of ionized, exospheric neutrals would be a major loss process at Titan, supplementing neutral and additional ionospheric escape. At that time, Titan was expected to be the most important source of new plasma in Saturn's magnetosphere. Results from the mission have so far shown that escape from Titan occurs, and is dominated by light ions, although heavy ions are also seen at times [e.g., *Hartle et al.*, 2006; *Coates*, 2009]. The pickup ion production rate from Titan's exospheric neutrals was estimated at $\sim$5 $\times$ 10^{22} ions s^{-1} [*Sittler et al.*, 2005, 2009], which as shown here is small compared to the ionospheric loss rate along Titan's tail. The overall loss rate was estimated at $\sim$1 $\times$ 10^{25} ions s^{-1} based on Radio and Plasma Wave Science investigation (RPWS) Langmuir Probe data [*Wahlund et al.*, 2005], which neither makes differential energy measurements nor has mass discrimination. Using CAPS ion data, *Sittler et al.* [2010]

[1]Mullard Space Science Laboratory, University College London, London, UK.
[2]Centre for Planetary Sciences at UCL/Birkbeck, London, UK.
[3]Southwest Research Institute, San Antonio, Texas, USA.
[4]Los Alamos National Laboratory, Los Alamos, New Mexico, USA.
[5]Department of Physics and Astronomy, University of Montana, Missoula, Montana, USA.
[6]NASA Goddard Space Flight Center, Greenbelt, Maryland, USA.
[7]School of Engineering and Applied Science, University of Virginia, Charlottesville, Virginia, USA.
[8]Wigner RCP, RMKI, Budapest, Hungary.

Corresponding author: A. J. Coates, Mullard Space Science Laboratory, University College London, London RH5 6NT, UK. (ajc@mssl.ucl.ac.uk)

0148-0227/12/2012JA017595

estimated an ionospheric loss rate of $\sim 4 \times 10^{24}$ ions s^{-1} for T9.

[5] Meanwhile, the most prolific source of plasma in Saturn's system is actually the moon Enceladus and the associated neutral particle cloud emanating from the Cassini-discovered plumes there [e.g., *Smith*, 2010], as well as from Saturn's rings [*Tseng et al.*, 2010; *Elrod et al.*, 2012]. A comparison of mass loading rates at different objects in the solar system, including Titan and Enceladus, was given by *Coates* [2012]. Additional escape mechanisms may include hydrodynamic escape, mass ionospheric escape as seen at Mars and Venus, as well as escape from the exosphere [*Johnson et al.*, 2009].

[6] One interesting result was the observation of ionospheric plasma in Titan's tail, several Titan radii (R_T) away from its source in the sunlit ionosphere, during the T9 encounter [e.g., *Coates et al.*, 2007; *Szego et al.*, 2007; *Wei et al.*, 2007; *Modolo et al.*, 2007a; *Bertucci et al.*, 2007; *Sittler et al.*, 2009, 2010]. During T9, the incoming flow direction differed somewhat from the corotation direction. A number of other encounters also reveal ionospheric photoelectrons in the tail [e.g., *Wellbrock et al.*, 2012; *Edberg et al.*, 2011], while a similar process is also present at Venus, Mars and Earth [*Coates et al.*, 2011b]. It was suggested that photoelectron escape would set up an ambipolar electric field promoting further escape from Titan [*Coates et al.*, 2007; *Sittler et al.*, 2009], in a process analogous to the Earth's polar wind [*Ganguli*, 1996].

[7] In addition, the T9 tail encounter provided abundant evidence for a split tail with two distinct ionospheric regions [e.g., *Coates et al.*, 2007; *Szego et al.*, 2007; *Wei et al.*, 2007; *Modolo et al.*, 2007a; *Bertucci et al.*, 2007]. This has been studied in simulations, some of which also (1) indicated a dual tail feature [*Modolo et al.*, 2007b; *Kallio et al.*, 2007; *Simon et al.*, 2007], (2) indicated a magnetic connection to the day and night side from the two regions [*Modolo et al.*, 2007b], (3) discussed the relation to Alfven wings [*Kallio et al.*, 2007], and (4) showed that Hall MHD provided a better fit to the data [*Ma et al.*, 2007]. Recent simulations by *Lipatov et al.* [2012] confirmed that the split tail may be associated with Alfven wings and ions moving along the field although a polarization electric field may also be important [*Lipatov et al.*, 1997]. Here, we report new evidence for a split tail geometry, also seen in the magnetometer and RPWS data (H.Y. Wei et al., manuscript in preparation, 2011) for the additional tail encounters T75 and T63.

[8] The geometry of Cassini's distant (5,000–10,000 km) tail encounters, and observations of the escaping ionospheric plasma, allow us, in this paper, to estimate the amount of plasma escape via this mechanism. We use the distinctive energy spectrum of ionospheric photoelectrons including the peak at 24.1 eV [*Coates et al.*, 2007; *Wellbrock et al.*, 2012; *Coates et al.*, 2011b, and references therein] to identify ionospheric plasma in the tail. We also examine the composition of the escaping plasma by analyzing the associated low energy ion data.

2. Instrumentation and Encounter Geometries

[9] The Cassini Plasma Spectrometer (CAPS) has been fully described elsewhere [*Young et al.*, 2004]. Here, we use data from the Electron Spectrometer (ELS) [*Linder et al.*, 1998] and the Ion Mass Spectrometer (IMS). The ELS measures the energy per charge of negatively charged species in an E/q range 0.6–28,750 eV/q, with a $\Delta E/E$ of 16.7%. The field of view is a 160° fan divided into 5° × 20° angular sectors. This can be moved by the CAPS actuator allowing up to 1.8π sr angular coverage from the 3-axis stabilized Cassini spacecraft. Spectra are measured by converting counts from the microchannel plate detector, to phase space density and other physical units [*Lewis et al.*, 2008, 2010]. The IMS has a similar angular field of view and energy resolution, but the E/q range is 1–50280 eV. IMS also includes a linear electric field time of flight (TOF) ion mass identification system, from which m/q spectra and m/q-separated moments (for protons, m/q = 2 ions, m/q = 16 ions) may be derived numerically [*Thomsen et al.*, 2010]. We use these data here in the upstream regions away from those which include ionospheric plasma.

[10] Within the observed ionospheric ion outflow regions themselves, we use time of flight (TOF) data to analyze separately masses m/q = 1, 2, 16 and 28, and we estimate their velocities using 1-D Maxwellian fits to the energy spectra in the TOF data. We also determine the density for each species from the TOF data, and normalize these to the total density from the numerical moments for each species. In this mass separation, m/q = 1 indicates protons, m/q = 2 indicates H_2^+ or much less likely He^{++}. The presence of oxygen as part of the observed heavier species is specifically excluded as there is no O^- peak in the TOF spectra, which would be present from oxygen-bearing molecules. The m/q = 16 population could also include contributions from m/q 17 and 18, while m/q = 28 could include species up to m/q = 32. The possibilities include CH_4^+ and N_2^+ for m/q = 16 and 32 respectively, but the identifications are not definitive for these species. We can, however, definitely rule out oxygen-bearing species for both the m/q = 16 and 28 populations as no O^- population is seen in the IMS 'straight through' (ST) data. We also note that modeling shows that ion distributions may be more complex than simple Maxwellians [*Lipatov et al.*, 2011].

[11] A schematic illustration of the T9, T75 and T63 encounter geometries is shown in Figure 1. In this plot, three projections of Titan's position and the Cassini flyby trajectories are shown, in a system with Titan itself at the origin. The spacecraft trajectories begin at the diamond in each case and are shown for ±1 h from closest approach, with 10 min tick marks. We use a coordinate system where the +*y* axis is directed into the corotating flow (with −y along the corotation wake), +x points toward Saturn, and +z points North of the equator, completing the right-handed set. While as mentioned above there are deviations from this nominal configuration, this nevertheless provides a useful framework for comparing encounters. In this frame, the nominal electric field ($\boldsymbol{E} = -\boldsymbol{v} \times \boldsymbol{B}$) points anti-Saturnward along −x, and the Sun direction is indicated by lines from Titan (see caption).

[12] Figure 1 shows that the T9, T75 and T63 geometries are quite similar in orientation with respect to the corotation wake, with T63 somewhat closer to Titan. The T9 geometry is nearly the same as that for T75. The parameters for all

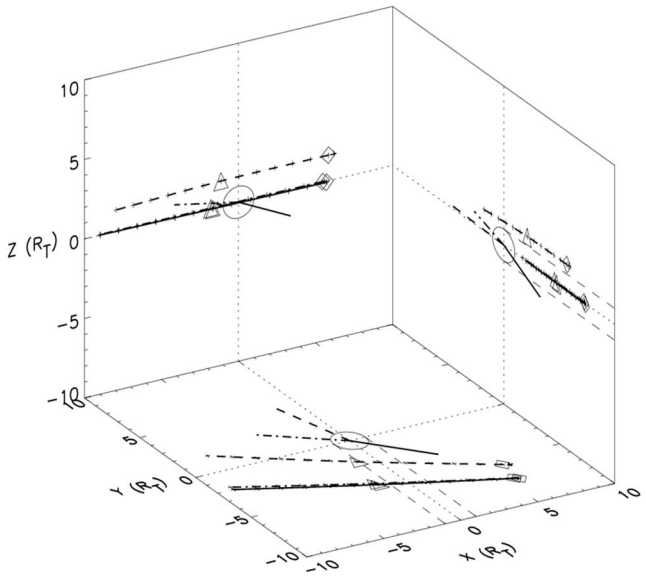

Figure 1. Geometry of the T9 (solid line), T75 (dot-dashed line) and T63 (dashed line) encounters; T75 and T9 are almost identical in this plot. The Cassini trajectory (starting at the diamond symbols) is shown for closest approach (shown as triangles) ±1 h, with 10 min tick-marks in each case. The lines from the center of Titan show the Sun direction in each case.

three encounters are summarized in Table 1, together with information about the upstream conditions in each case (see following sections).

3. T9

[13] We first summarize the CAPS data from the T9 encounter, where ionospheric plasma was seen in two intervals along the tail [*Coates et al.*, 2007; *Szego et al.*, 2007; *Coates*, 2009; *Sittler et al.*, 2010]. During interval 1 (~18:25:30–18:45 UT), ionospheric photoelectrons were seen at 6.8–5.4 Titan radii (R_T) in the distant tail, indicating plasma escape and a magnetic connection to the sunlit ionosphere. Heavy ions were seen escaping in this interval.

[14] During interval 2 (~19:10:30–19:30 UT), a mixed population of ionospheric and magnetospheric plasma was seen in the electron and ion data. Light ions were the dominant species in this case. Trace populations with M/Q ~ 16 were identified during interval 2 [*Sittler et al.*, 2010], which could be either low energy pickup CH_4^+ ions or ionospheric CH_5^+ ions. Spectrogram data from T9 are shown in the top two panels of Figure 2, for electrons and ions respectively.

[15] As mentioned above, it was suggested that an ambipolar electric field may be set up by the escaping relatively energetic photoelectrons to drive the ion escape in a mechanism similar to Earth's polar wind. Also, *Coates et al.* [2007] suggested that lower-mass ions were from a higher altitude in the ionosphere. *Sittler et al.* [2010] suggested that the different composition may rather be due to different parts of the upstream plasma disk. There is support for both of these ideas from simulations [e.g., *Modolo et al.*, 2007b; *Lipatov et al.*, 2012] showing that both effects may be important.

[16] To estimate the escape rate Q (ions s^{-1}) we require the product

$$Q = c\, n_{ELS}\, v\, A$$

where $c = 5.2 \times 10^{21}$ ($cm^3\ km^{-1}\ R_T^{-2}$) is a constant for units conversion, n_{ELS} is the density in cm^{-3} determined from ELS (having taken spacecraft potential into account), v is the ion velocity relative to Titan in km/s and A is the area (πR_T^2) determined from the width of the tail crossing ($1R_T$ = 2575 km). In reality this may provide an upper limit due to more complex (but smaller) shapes being possible (see discussion section).

[17] First, we estimate the plasma density from ELS. In order to do this, a spacecraft potential is needed in the analysis. In the upstream region away from intervals 1 and 2 (see Figure 2, first panel), when low energy photoelectrons from the spacecraft are visible in ELS, the positive spacecraft potential is determined from ELS observations using the upper energy of the observed spacecraft photoelectrons, and then used to determine the densities in the upstream region. However, during the higher density ionospheric plasma interval 1, it is likely that spacecraft potential is zero or slightly negative even at this large distance from Titan. Similar potentials are observed during most passes through Titan's ionosphere (e.g., −1 V as determined from the Langmuir probe during TA [*Wahlund et al.*, 2005]) and here the ELS data look clearly ionospheric, since the ionospheric photoelectron peak is certainly visible [see *Coates et al.*, 2007; *Coates*, 2009]. The measured energy of the observed ionospheric photoelectron peak during interval 1 is ~22.1 eV (see spectra presented in *Coates et al.* [2007]). Theoretically, an energy of 24.1 eV is expected from photoelectron production by 30.4 nm solar radiation impacting on Titan's ionosphere [see *Coates et al.*, 2011b, and references therein]. This is due to the $A^2\Pi_u$ transition in N_2. The 2 eV difference between the observed and predicted photoelectron energies allows us to determine a negative spacecraft potential of −2V from ELS in this case. A spacecraft potential of −2V is further supported by representative Spacecraft-Plasma Interactions System (SPIS, see http://dev.spis.org/projects/spine/home/spis) simulations (not shown).

Table 1. Summary of Encounters Used Here

Encounter	Date	Time (UT)	Altitude (km)	Saturn Local Time	Classification [cf. *Rymer et al.*, 2009]	Upstream Velocity (% Corotation, Deviations)
T9	26 Dec (day 360) 2005	18:59	10411 (tail)	03:03–03:05	Plasma sheet	81, Southward flow
T75	19 Apr (day 109) 2011	05:00	10053 (tail)	14:14–14:16	Lobe/Plasma sheet	72
T63	12 Dec (day 346) 2009	01:03	4850 (tail)	16:57–16:59	Plasma sheet/Lobe	96

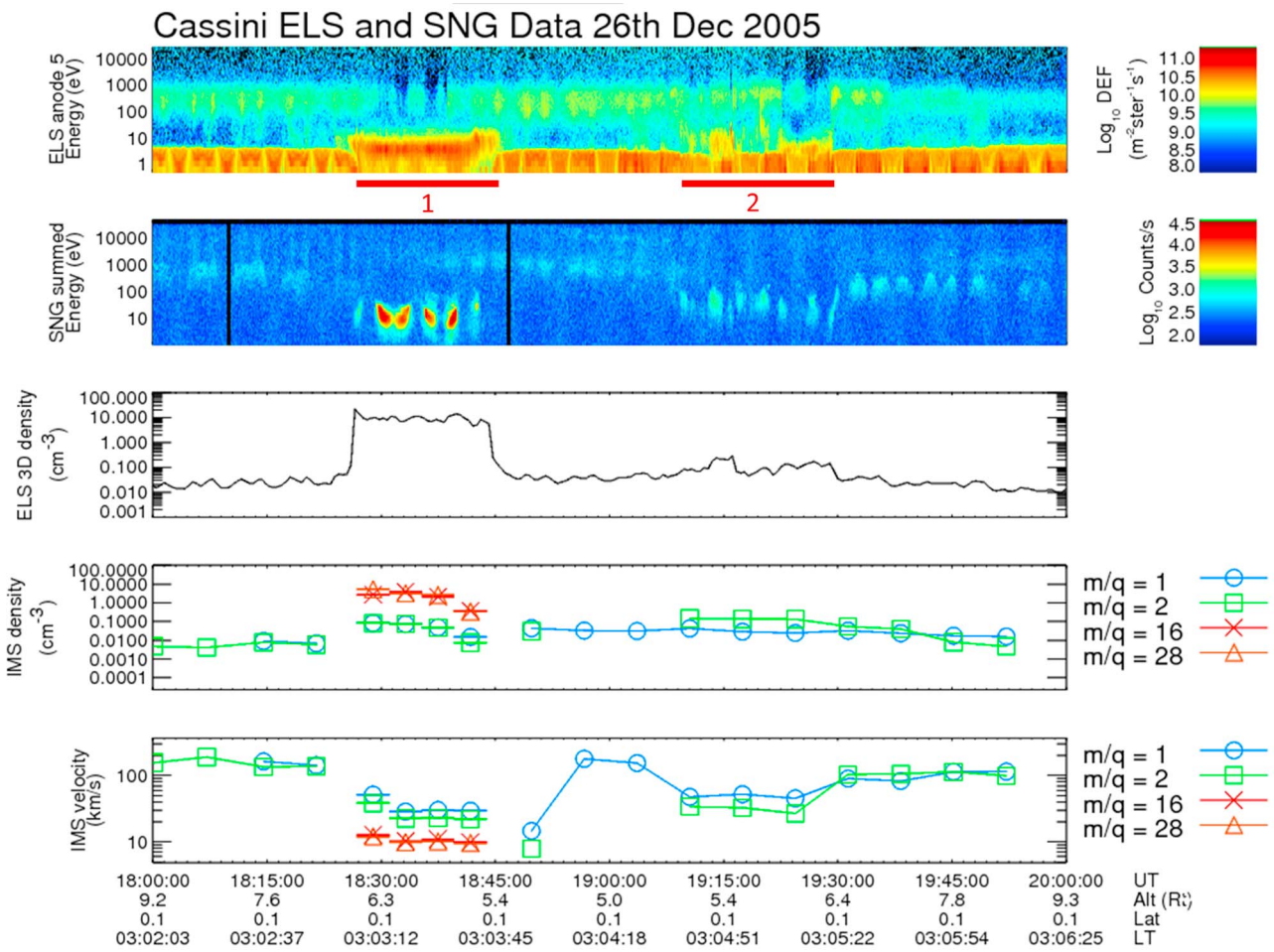

Figure 2. Composite plot of CAPS electron and ion data during T9. First panel shows the ELS spectrogram from Anode 5, second panel shows the IMS singles spectrogram averaged over all anodes, and third panel shows the density determined from ELS data (see text). Fourth and fifth panels show the density and velocity calculated from IMS numerical and TOF-based moments (see text).

[18] During interval 1, we use the spacecraft potential of −2V, and 'fill in' the unobserved region of phase space between the spacecraft potential and 0 V (in the spacecraft frame), with a linear extrapolation of phase space density (determined in a frame shifted to the spacecraft potential, according to Liouville's theorem). This then gives a density of ∼10 cm^{-3} from ELS, which is in good agreement with the densities derived from the ion moments, and also with the density in the same interval determined from the RPWS Langmuir probe [*Modolo et al.*, 2007a; *Wei et al.*, 2007, Figure 3]. A time series of the density results is shown in the third (ELS) and fourth (IMS) panels of Figure 2. In Panels 4, the IMS density data away from intervals 1 and 2 is estimated from numerical moments, and in regions 1 and 2 we show results from the TOF separation technique, as described above.

[19] For the speed determination, we have a number of possibilities. First, we assume a plasma flow speed equal to the corotation speed, providing an upper limit for our escape rate estimates. We note that the escaping ion bulk velocity will be less than this due to kinetic effects. For T9 we use an area with diameter 1.7 R_T in Interval 1 for all the estimates. This gives an ion escape rate of $\sim 3.1 \times 10^{25}$ ions s^{-1} for interval 1 (normalized and listed under '$V_{corotation}$' in Table 2), though different escaping masses are not separated at this point. As for the ion densities, the observed ion velocities in the region upstream of Titan are given by the CAPS numerical ion moment calculations from IMS [*Thomsen et al.*, 2010], while in Titan's ionosphere the ions are separated into light ions (H^+ and H_2^+) and mass 16 (likely to be CH_4^+) and 28 (likely to be N_2^+) based on TOF data analysis. This gives the density fraction and velocity for each species (see fuller description above). The results of these calculations are shown in the fifth panel of Figure 2, and are very close to those reported by *Sittler et al.* [2010], who use a similar velocity moment algorithm. If we use the observed ion speed from the numerical moments for T9 away from closest approach (∼170 km/s) we obtain 2.6×10^{25} ions s^{-1} (species not separated - normalized and listed under '$V_{observed}$' in Table 2). If instead we use the average observed ion energy (species again not separated) for the escaping ions (determined from the second panel of Figure 2), we then estimate $\sim 1.1 \times 10^{25}$ ions s^{-1} assuming all the ions are H^+, 2.9×10^{24} ions s^{-1} assuming m/q = 16, or 1.6×10^{24} assuming the ions are m/q = 28. These values are normalized

Table 2. Escape Rate Estimates, Divided by 1×10^{23} Ions s^{-1} for Clarity (amu s^{-1} in Last Column)[a]

Encounter	$V_{corotation}$	$V_{observed}$	E_{esc} H^+	E_{esc} m/q = 16	E_{esc} m/q = 28	V_{esc} m/q = 1–2	V_{esc} m/q = 16	V_{esc} m/q = 28	Total	Mass Loss (amu s^{-1})
T9	310	260	110	29	16	1	14	14	**42**	**890**
T75	21	15	9	2	1	1	2	2	**10**	**160**
T63	95	91	35	9	5	2	5	5	**23**	**400**

[a]The $V_{corotation}$ and $V_{observed}$ columns contain estimates based on the corotation and observed plasma flow speeds respectively, the E_{esc} columns are estimated using the observed energy of escaping ions for different m/q assumptions, and the V_{esc} columns are estimated using the observed ion velocities and m/q determinations. The totals in the last two columns (in bold) include both observed intervals in each case, and indicate the total ion and mass loss rates from Titan.

and listed under 'E_{esc}' for the different m/q assumptions in Table 2.

[20] A more precise estimate may be made using the observed ion velocities of the escaping population from the species-separated IMS moments (fifth panel of Figure 2). These give rates of 1.2×10^{23} for m/q = 1–2, 1.4×10^{24} ions s^{-1} for m/q = 16 and 1.4×10^{24} ions s^{-1} for m/q = 28. The total loss rate is then 2.8×10^{24} ions s^{-1} corresponding to a mass loss rate of 6.0×10^{25} amu s^{-1}. These values are normalized by a factor 1×10^{23} and listed under 'V_{esc}' for the different m/q determinations in Table 2.

[21] The latter estimates, valid in Interval 1, will be supplemented by escaping particles in region 2 where intermittent ionospheric plasma spectra are observed as indicated by the intermittent nature of the ionospheric photoelectrons in Interval 2. We estimate that Interval 2 would add another ~50% based on the intermittent ionospheric plasma, bringing our totals to 4.2×10^{24} ions s^{-1} or 8.9×10^{25} amu s^{-1}, during T9. These values are normalized and listed under 'Total' and 'Mass loss' respectively in Table 2.

[22] For comparison, *Sittler et al.* [2010] did not consider the contribution from light ions in interval 1. However, they did identify the dominant ions as m/q ~17 and ~29, and estimated a total ion density ~8 cm^{-3} in interval 2, giving a calculated ionospheric loss rate of $\sim 4 \times 10^{24}$ ions s^{-1}, which is very similar to ours.

[23] The escape rate estimates from all techniques discussed here are shown in Table 2, where the rates are normalized to multiples of 1×10^{23} ions s^{-1} (or amu s^{-1} for the mass loss column), for ease of comparison.

[24] The composition data presented in the fourth panel of Figure 2 confirm that interval 1 is dominated by heavy ions and interval 2 by light ions, in agreement with *Coates et al.* [2007], *Szego et al.* [2007], and *Sittler et al.* [2010].

[25] In addition, we note that in the region upstream of Titan the velocity component in the corotation direction (not shown) is dominant, although from inspection of velocity data (not shown) there is a significant Southward component in the T9 case [cf. *Szego et al.*, 2007]. Furthermore, the magnetic field orientation is almost in Titan's equatorial plane [*Bertucci et al.*, 2007]. The corotational velocity component corresponds to ~81% of the corotation speed. The upstream conditions for T9 were classified by *Rymer et al.* [2009] as 'plasma sheet' like. However, the composition in the upstream region is principally protons. Some of these upstream region conditions are summarized in Table 1.

4. T75 Data

[26] CAPS data from T75 are shown in Figure 3 as a composite plot, in a similar format to Figure 2. As well as the geometry being similar to T9 (see Figure 1), the electron data again show multiple tail-like populations of relatively dense, cold plasma. Two intervals are indicated on Figure 3. During these intervals, dense, low energy plasma is seen which appears ionospheric. Further evidence of ionospheric photoelectron peaks is seen in the individual spectra shown in Figure 4. Simultaneously, in both intervals 1 (~04:21–04:33 UT) and 2 (~04:48–04:57 UT), we also note that there are clear separate populations of magnetospheric plasma in addition to the ionospheric population. During intervals 1 and 2, the ion population also shows a clear decrease to lower energies. It is also clear that the composition of the magnetospheric plasma is devoid of heavy ions, which indicates that Titan is outside the magnetospheric plasma sheet for most of the encounter period, re-entering it at ~05:32 UT.

[27] Figure 3 (third panel) shows the electron densities calculated using a spacecraft potential estimated either from the observed spacecraft photoelectrons (when positive), or determined from the observed ionospheric photoelectron peak or feature in the spectrum when the spacecraft photoelectrons are absent, as in the case of T9. In this case, a spacecraft potential of 0 V was adopted. Although this technique is somewhat inaccurate, the calculated density of escaping plasma reaches an upper limit of ~1.5–2 cm^{-3} in this case, in fair agreement with RPWS upper hybrid frequency data (Wei et al., manuscript in preparation, 2011).

[28] In Figure 3 (fourth and fifth panels), we show the ion numerical moments away from intervals 1 and 2 and the TOF-derived moments during intervals 1 and 2. In Figure 4 we show selected electron spectra observed during intervals 1 and 2. Although such spectra are intermittent and not present in every sample, there is a change of slope at ~23–24 eV, corresponding to the anticipated line feature in the ionospheric photoelectron spectrum. When present, they are again evidence of magnetic connection to their production region in the dayside ionosphere, and they provide further evidence that the observed plasma is of ionospheric origin. The location in the spectrum is consistent with the adopted spacecraft potential of 0 V here.

[29] As with the T9 data, we now use the observed density and corotation velocity to infer the plasma escape rate. Using similar assumptions as before, including the observed width of Interval 1 (1.4 R_T), gives a rate of $\sim 2.1 \times 10^{24}$ ions s^{-1} using the corotation speed assumption. Using the measured velocity magnitude upstream of Titan for IMS data gives 1.5×10^{24} ions s^{-1}. This reduces to $\sim 9.0 \times 10^{23}$ ions s^{-1} for H^+, 2.2×10^{23} ions s^{-1} for m/q = 16 and 1.3×10^{23} ions s^{-1} for m/q = 28, using the measured ion energy to estimate the streaming velocity with respect to Titan.

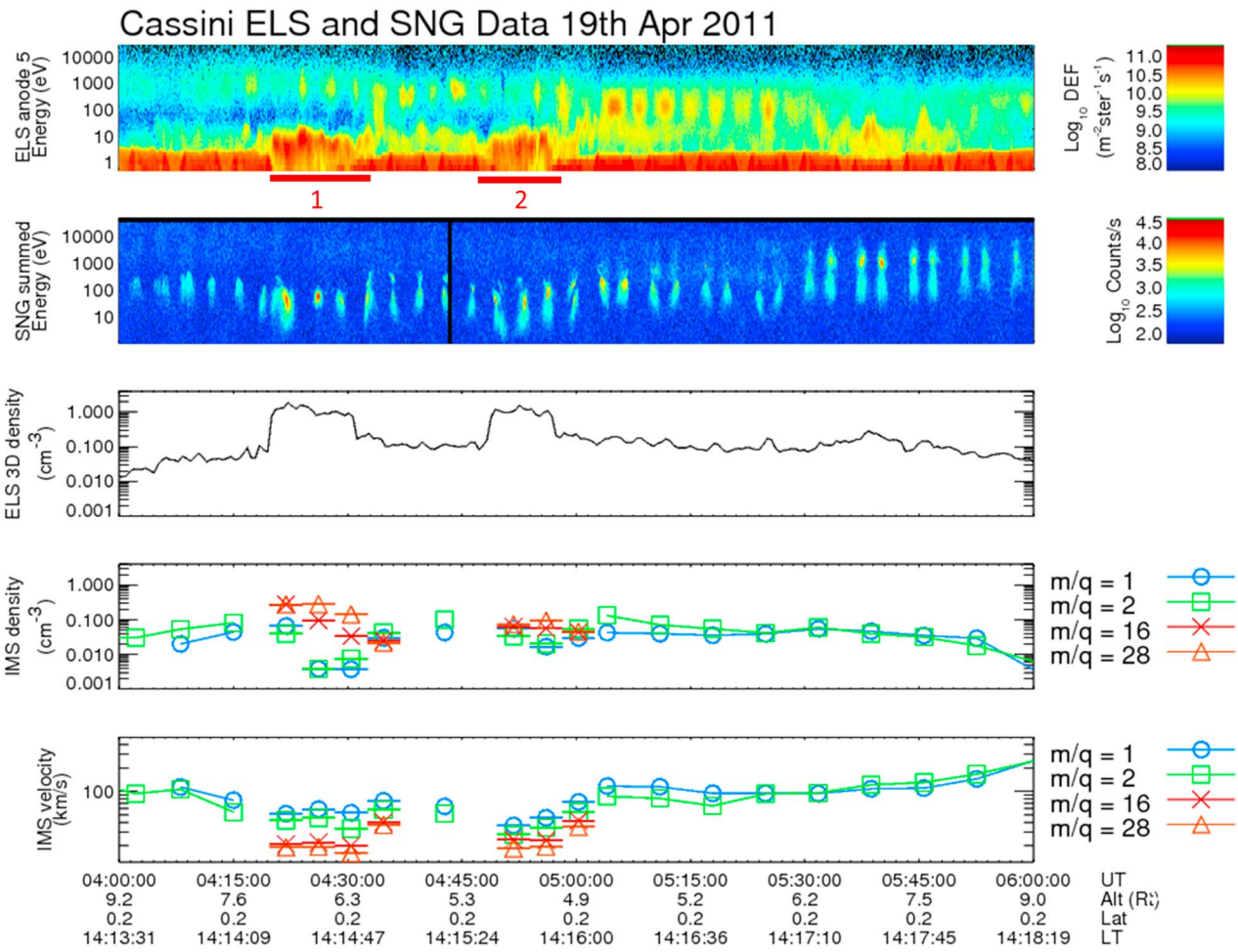

Figure 3. Composite plot of CAPS electron and ion data during T75, in a format similar to Figure 2.

[30] If we use the measured velocity of the escaping ions to estimate this streaming speed, in this case we get values of 1.4×10^{23} ions s^{-1}, 1.5×10^{23} ions s^{-1} and 1.8×10^{23} ions s^{-1} for m/q = 1–2, m/q = 16, and m/q = 28 respectively, giving total loss rates of 4.8×10^{23} ions s^{-1} and 7.7×10^{24} amu s^{-1}. Here, intervals 1 and 2 are quite similar, and we estimate that the total loss rate would approximately double to 9.6×10^{23} ions s^{-1} and the mass loss rate is 1.6×10^{25} amu s^{-1}. Again the rate information is summarized in Table 2, where the totals are calculated from the estimates from the measured velocities and include both intervals 1 and 2.

[31] In contrast to the T9 case, T75 composition data (fourth panel in Figure 3) reveals mixed composition with dominant heavy ions during interval 1, and similar light and heavy densities of escaping ions during interval 2. The velocity data outside intervals 1 and 2 indicate dominance by the corotational velocity component in the region upstream of Titan. The magnetic field orientation (Wei et al., manuscript in preparation, 2011) is relatively dipolar. The corotational component corresponds to ~72% of the corotation speed. The T75 upstream conditions correspond to lobe-like inbound, and plasma sheet outbound, conditions according to the classification system of *Rymer et al.*, 2009. Again, the composition in the upstream region is principally protons. Some of these upstream region conditions are summarized in Table 1.

5. T63 Data

[32] Data from T63 are shown in Figure 5, with the electron spectrogram in the first panel. Remarkably, in this case again a dual tail structure is observed. During both intervals 1 (~00:19:30–00:34:30 UT) and 2 (~00:52:30–01:11:30 UT), both ionospheric and magnetospheric electrons are seen (first panel); however, the latter are less intense during interval 2. Also noticeable in Figure 5 (second panel) is a narrow (in energy and angle) population of ions seen between ~01:00–01:40 UT, rising in energy with time. This is likely to be a population of pickup ions from Titan similar to the observation of narrow features with m/q~1 from Titan's extended exosphere and (sometimes) m/q = 16,28 during TA [*Hartle et al.*, 2006] and T18 [*Sittler et al.*, 2010].

[33] Figure 5 (third panel) shows the density calculated from ELS. For the dense regions where a spacecraft potential is below the ELS energy range and cannot be determined from the spacecraft photoelectrons, a potential of −0.5 V is adopted consistent with the spectral data in Figure 6. This is also consistent with the potential determined for earlier encounters where similar low energy spectra are seen (TA

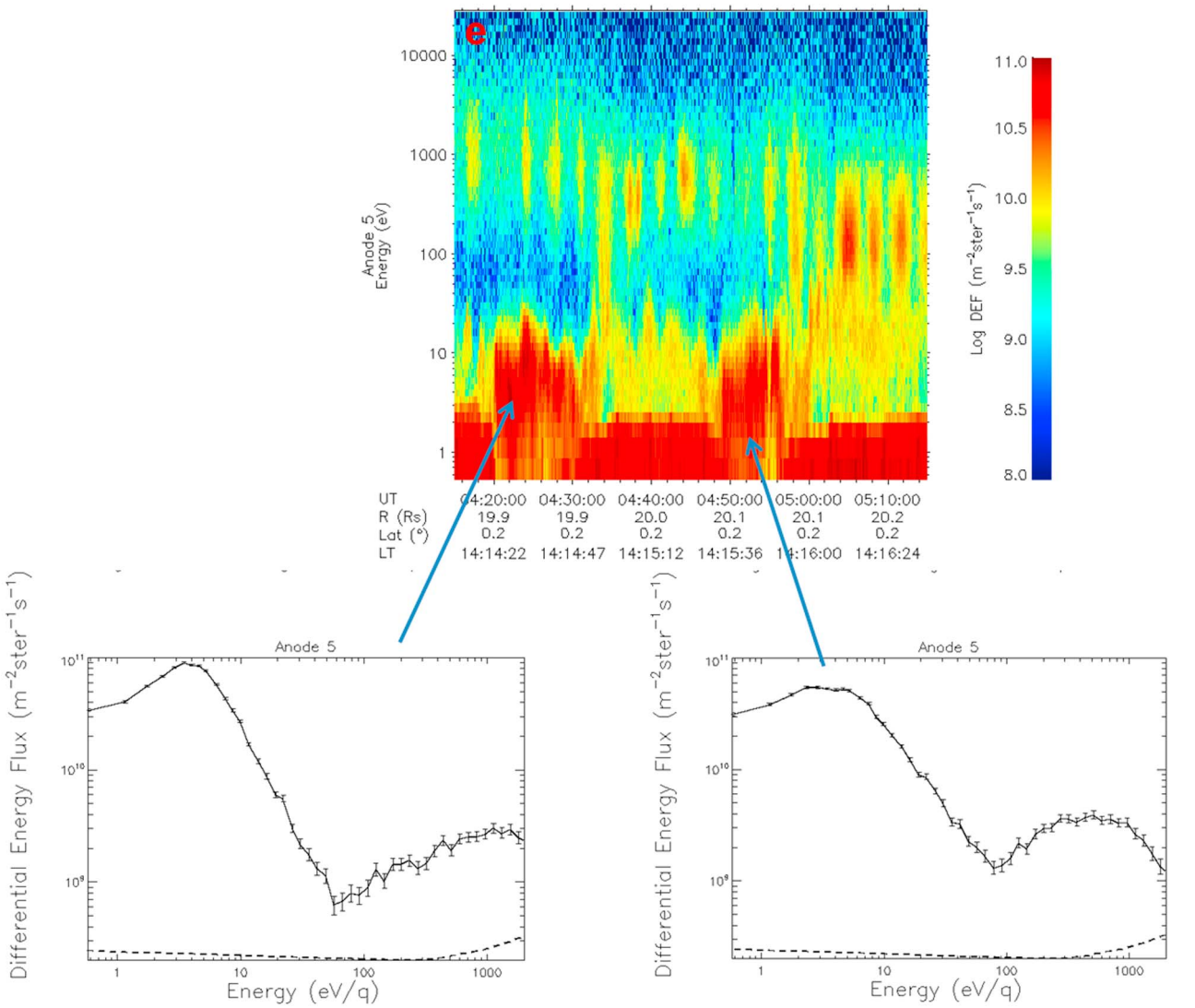

Figure 4. Electron spectra during T75.

[e.g., *Coates*, 2009; *Wahlund et al.*, 2005]). Figure 5 (fourth and fifth panels) show the ion numerical moments away from intervals 1 and 2, and TOF-derived moments within intervals 1 and 2. Figure 6, similar to Figure 4, shows selected spectra during the two intervals of interest. As for T75, such spectra again show a ledge corresponding to the 24.1 eV ionospheric photoelectrons which are similarly intermittent as they were during T75.

[34] We may use these data to estimate escape rates, including the observed width of interval 1 (2.09 R_T for T63)., Using the observed density and corotation velocity gives 9.5×10^{24} ions s^{-1}. Using the measured upstream ion velocity gives 9.1×10^{24} ions s^{-1}. Using the observed escaping ion energy gives 3.5×10^{24} ions s^{-1}, 8.7×10^{23} ions s^{-1} and 4.9×10^{23} ions s^{-1} for H^+, m/q 16 and m/q 28 respectively.

[35] Using the measured ion velocity yields more accurate values, of 2.3×10^{23} ions s^{-1} for m/q = 1–2, 4.5×10^{23} ions s^{-1} for m/q 16, and 4.5×10^{23} ions s^{-1} for m/q 28, giving a total loss rate of 1.1×10^{24} ions s^{-1}. The corresponding mass loss rate is 2.0×10^{25} amu s^{-1}. As in T75, these are only for interval 1, and we estimate that the similar interval 2 would increase the numbers to a total rate of $\sim 2.3 \times 10^{24}$ ions s^{-1} and a mass loss rate of 4.0×10^{25} amu s^{-1}.

[36] During T63, the composition data (fourth panel of Figure 5) shows that intervals 1 and 2 are both dominated at times by heavy ion escape. Again, the velocity data (not shown) indicate that the component in the corotation direction is dominant in the region upstream of Titan. The magnetic field orientation (Wei et al., manuscript in preparation, 2011) is relatively dipolar. The corotational component corresponds to ~96% of the corotation speed. The T63 upstream conditions correspond to plasma sheet inbound and lobe like outbound according to the classification of *Rymer et al.*, 2009. Again, the composition in the upstream region is principally protons. Some of these upstream region conditions are summarized in Table 1.

6. Discussion

[37] Clearly, the density of ionospheric plasma observed in the tail can yield important information about charged

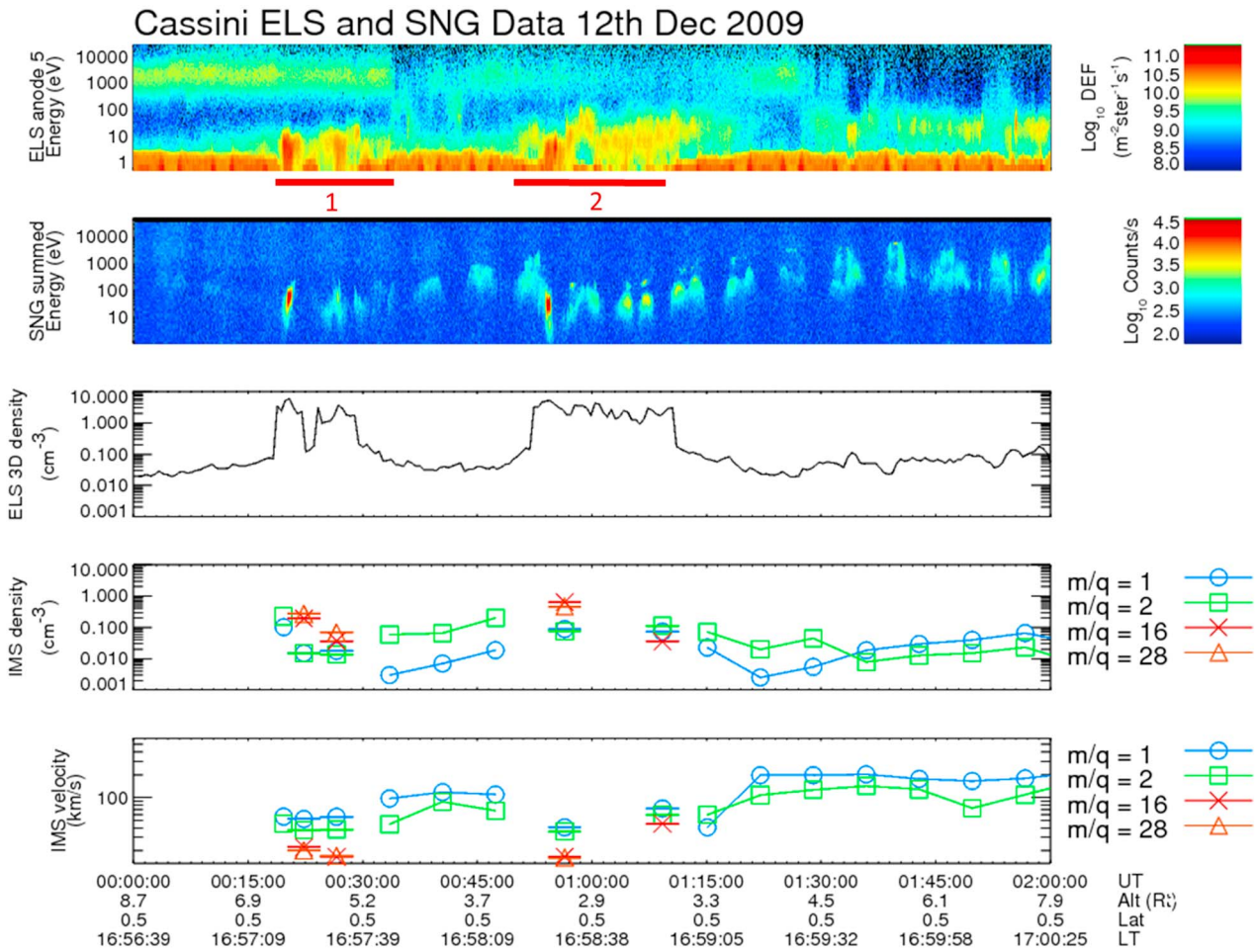

Figure 5. Composite plot of CAPS electron and ion data during T63, in a format similar to Figure 2.

particle escape rates from Titan's environment. The observed ion velocities probably give the best estimate of the overall rate. Because of their low energy and narrow energy distributions, we infer that the ions were formed in the ionosphere and swept along field lines out of Titan's atmosphere. We distinguish them from what we refer to as 'pick-up' ions (particularly visible during T63) that are also swept away but are ionized in an extended exospheric region where the flow velocity is significant and they acquire significant gyrational energy. These have not been included in our estimates due to the difficulty of their observation as all filled parts of their ring distribution may not be observed simultaneously by IMS. The pickup ions discussed by *Sittler et al.* [2010] for T18 could be due to Titan's extended H_2 exosphere. They are almost certainly present during the other encounters presented here, but the limited field of view of IMS and the ring-like, and probably nongyrotropic [e.g., *Coates et al.*, 1993] nature of their distribution function unfortunately precludes their observation on a routine basis.

[38] The neutral and ion escape processes at Titan were reviewed by *Johnson et al.* [2009]. The mechanisms include thermal escape, chemically induced escape, slow hydrodynamic escape, pickup ions and ionospheric outflow, and plasma-induced sputtering. In this paper, we have estimated the total escape of low energy plasma but omit higher energy populations including pickup ions as mentioned above. The estimates presented here are therefore a lower limit for the total escape flux.

[39] In addition, several assumptions are made in the analysis, for example the approximation of cylindrical escape channels with area A. With observations along the trajectory, this is probably the best approximation for which we estimate an error of ~50% based on simulations. Looking at comparisons with simulations, the escape channels may well have more complex shapes [e.g., *Ma et al.*, 2006; *Modolo et al.*, 2007b; *Snowden et al.*, 2011] as well as non-uniform densities within the escape regions (as shown by the variations in density in Figures 2, 3, and 5).

[40] Our density calculation also requires estimation of spacecraft potential. In the case of T9 and T75 this was reasonably well constrained by using the observed energy of ionospheric photoelectrons. In addition, our density values are in good agreement with other estimates for T9 [*Wei et al.*, 2007] and for T75 (Wei et al., manuscript in preparation, 2011). For T63 however, the spacecraft potential value adopted was used because of similarity to other encounters such as TA. The possible error from this source is estimated at ~50% for T63 and < 20% for T9 and T75.

[41] Despite the various errors mentioned above, the estimates of overall escape flux in Table 2 are comparable with

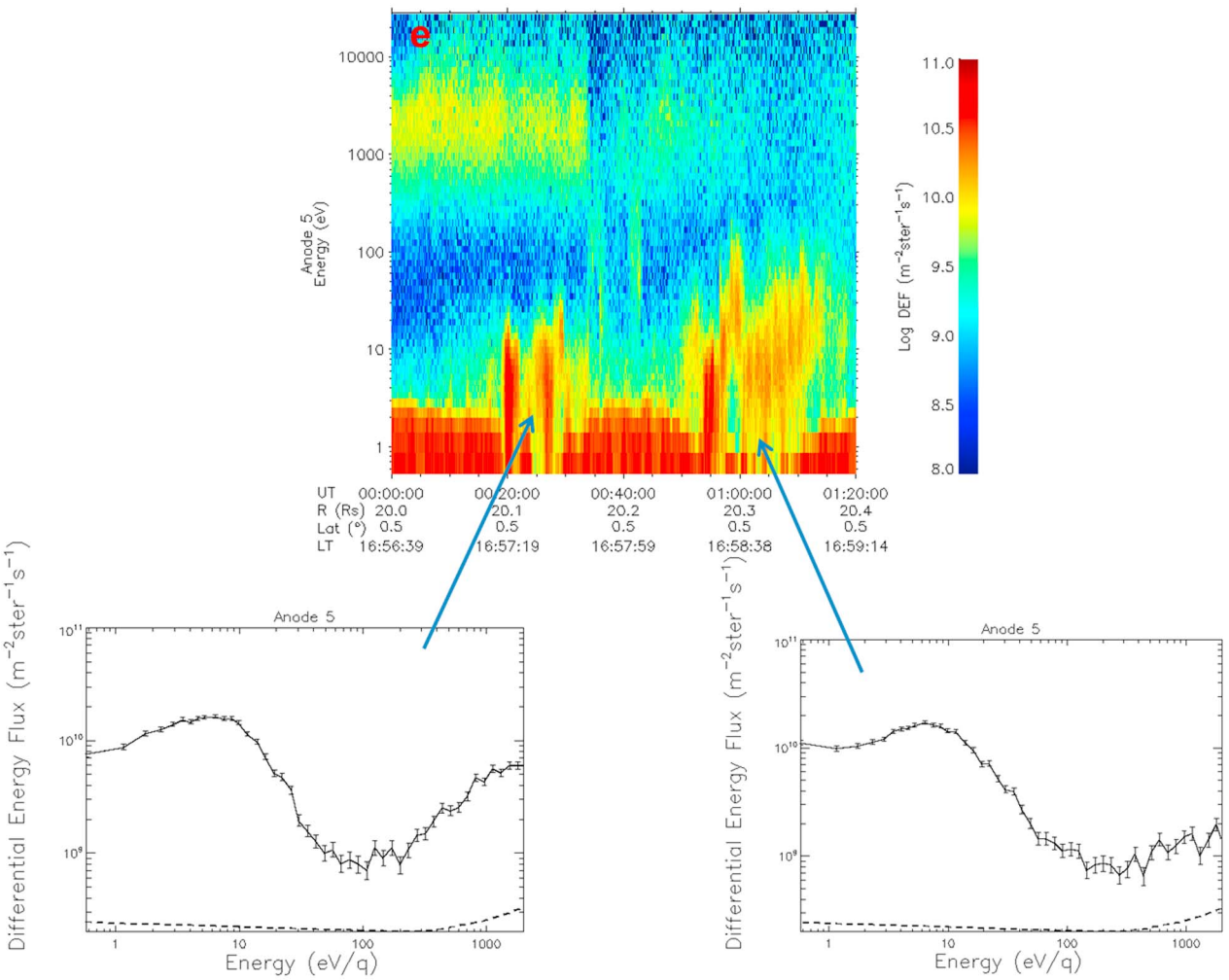

Figure 6. Electron spectra during T63.

modeling results [e.g., *Nagy et al.*, 2001; *Modolo et al.*, 2007b; *Sillanpää et al.*, 2006]. However, our estimates are a factor ~2 lower than other databased estimates from the TA encounter obtained using density and velocity estimates from the Langmuir probe [*Wahlund et al.*, 2005]. However, the TA encounter also occurred within the dayside plasma sheet, therefore energy input was higher from the upstream plasma environment which may have contributed to higher inferred fluxes. Our estimates for the T9 encounter are, however, in good agreement with those of *Sittler et al.* [2010], where similar methods are used. There are many approximations used to derive all the numbers in the previous estimates, but we suggest that the results presented here are the best constrained by observations.

[42] There are some variations in the escape rates between the encounters (Table 2). These are most likely associated with the approximations mentioned above, though there may also be real variations in the escape rate from Titan. Also, all of these encounters took place when Titan was outside the magnetospheric plasma sheet, as indicated by light ions dominating the magnetospheric composition. This will be the topic of further study.

[43] It is interesting to compare our observed plasma escape rates at Titan with those at other solar system bodies [e.g., *Coates*, 2012]. Escape rates at Mars and Venus were recently reviewed by *Lundin* [2011, and references therein]. At Mars, the updated escape rates were separated into different energy ranges: <200 eV (few $\times$ 10^{24} ions s^{-1}) and >200 eV (10^{23}–10^{24} ions s^{-1}), depending on distance into the tail [see *Lundin*, 2011, Figure 15]. At Venus, the observed rates by *Fedorov et al.* [2011] were 2.7 $\times$ 10^{24} ions s^{-1} for O^+ and 7.1 $\times$ 10^{24} for H^+. These were recalculated by *Lundin* [2011], resulting in rates which were a factor 4 higher, though even these were lower than those of *Brace et al.* [1982], possibly indicating the importance of solar cycle effects. The observed escape rates at Mars and Venus are thus comparable with our observed rates at Titan. Further work is clearly needed to understand the relative values in terms of planetary evolution.

7. Summary and Conclusions

[44] Other studies [*Coates et al.*, 2007, 2011b; *Wellbrock et al.*, 2012] have shown that photoelectrons are a key indicator of magnetic connection of dayside ionosphere, and may

be the extended ionosphere of Titan reaching into the tail. The three tail encounters studied here have some similarities between them in structure, with multiple intervals of ionospheric plasma in the tail. The ion measurements reported here support these findings from the plasma electron data, and photoelectron-driven escape provides one mechanism contributing to the total ion escape we observe. Our observations of electron distributions are important for comparison with hybrid and MHD modeling due to the importance of electron pressure in the Titan interaction.

[45] In the case of T9, plasma escape is seen along the tail, and there are two intervals of ionospheric plasma observed at several Titan radii, dominated by heavy and light ions respectively [see also *Coates et al.*, 2007; *Wei et al.*, 2007; *Szego et al.*, 2007; *Sittler et al.*, 2010]. Our estimated total measured escape rate is $\sim 4 \times 10^{24}$ ions s^{-1} and the mass loss rate is 9×10^{25} amu s^{-1}.

[46] For T75, which has very similar encounter geometry to T9, there are at least two intervals in the tail containing ionospheric plasma. A total escape rate of approximately 9.6×10^{23} ions s^{-1} and a mass loss of 1.6×10^{25} amu s^{-1} are seen in this case. During both intervals, there are intermittent photoelectron fluxes observed at several Titan radii, similar to interval 2 of T9. In interval 1, the composition is dominated by heavy ions, whereas in interval 2 the escaping plasma consists of a mixture of heavy and light ions. The split tail feature appears to be a common feature of Titan's interaction with Saturn's magnetosphere.

[47] The T63 encounter was closer to Titan than T9 or T75, and slightly polar with respect to the nominal corotation direction, but again two intervals of ionospheric plasma are seen at several Titan radii, in this case simultaneously with magnetospheric plasma. The escape rate calculation gives approximately 2.3×10^{24} ions s^{-1} and a mass loss rate of 4.0×10^{25} amu s^{-1}. During both intervals 1 and 2, the escape is at times dominated by heavy ions in this case.

[48] The variations in the escape rate noted here between the encounters may be due to uncertainties in estimation, or they may reflect real differences in the escape rate. Using an average rate of mass loss from the values found here, we find that $\sim$7 tonnes per day of ions are currently being lost from Titan's atmosphere and ionosphere; this is clearly a significant amount if it can be extrapolated to solar system timescales.

[49] We note again that photoelectrons observed in the tail are sensitive tracers of a magnetic connection to the dayside ionosphere, and are consistent with the observed field direction [*Wei et al.*, 2011] for all the encounters reported here (T9, T75, T63) [cf. *Coates et al.*, 2007, 2011a, 2011b; *Wellbrock et al.*, 2012]. Additional observations during other tail photoelectron intervals at Titan encounters T40, T17, T15 are reported by *Wellbrock et al.*, 2012.

[50] **Acknowledgments.** We thank MAG team members H. Wei and C.T. Russell for useful discussions. We thank L.K. Gilbert for software support. We acknowledge support of CAPS ELS science by STFC, and of the CAPS ELS operations and software team by STFC (to 2010) and by ESA via the UK Space Agency (from 2011). CSA was supported by an STFC Postdoctoral fellowship and GHJ by an STFC Advanced Fellowship. Work in the U.S. was supported by NASA JPL contracts 1243218 and 1405851 to the Southwest Research Institute. Work at Los Alamos was conducted under the auspices of the U. S. Department of Energy, with support from NASA's Cassini project.

[51] Masaki Fujimoto thanks the reviewers for their assistance in evaluating this paper.

References

Arridge, C. S., et al. (2011a), Upstream of Saturn and Titan, *Space Sci. Rev.*, *162*, 25–83, doi:10.1007/s11214-011-9849-x.

Arridge, C. S., N. Achilleos, and P. Guio (2011b), Electric field variability and classifications of Titan's magnetoplasma environment, *Ann. Geophys.*, *29*, 1253–1258, doi:10.5194/angeo-29-1253-2011.

Bertucci, C., F. M. Neubauer, K. Szego, J.-E. Wahlund, A. J. Coates, M. K. Dougherty, D. T. Young, and W. S. Kurth (2007), Structure of Titan's mid-range magnetic tail: Cassini magnetometer observations during the T9 flyby, *Geophys. Res. Lett.*, *34*, L24S02, doi:10.1029/2007GL030865.

Bertucci, C., et al. (2008), The magnetic memory of Titan's ionized atmosphere, *Science*, *321*, 1475–1478, doi:10.1126/science.1159780.

Blanc, M., et al. (2002), Magnetospheric and plasma science with Cassini-Huygens, *Space Sci. Rev.*, *104*, 253–346, doi:10.1023/A:1023605110711.

Brace, L. H., R. F. Theis, and W. R. Hoegy (1982), Plasma clouds above the ionopause of Venus and their implications, *Planet. Space Sci.*, *30*, 29–37, doi:10.1016/0032-0633(82)90069-1.

Coates, A. J. (2009), Interaction of Titan's ionosphere with Saturn's magnetosphere, *Philos. Trans. R. Soc. A*, *367*, 773–788, doi:10.1098/rsta.2008.0248.

Coates, A. J. (2012), Ion pickup and acceleration: Measurements from planetary missions, in *Physics of the Heliosphere: A 10-Year Retrospective*, *AIP Conf. Proc.*, in press.

Coates, A. J., A. D. Johnstone, B. Wilken, and F. M. Neubauer (1993), Velocity space diffusion and non-gyrotropy of pickup water group ions at comet Grigg-Skjellerup, *J. Geophys. Res.*, *98*, 20,985–20,994, doi:10.1029/93JA02535.

Coates, A. J., F. J. Crary, D. T. Young, K. Szego, C. S. Arridge, Z. Bebesi, E. C. Sittler Jr., R. E. Hartle, and T. W. Hill (2007), Ionospheric electrons in Titan's tail: Plasma structure during the Cassini T9 encounter, *Geophys. Res. Lett.*, *34*, L24S05, doi:10.1029/2007GL030919.

Coates, A. J., J.-E. Wahlund, K. Ågren, N. Edberg, J. Cui, A. Wellbrock, and K. Szego (2011a), Recent results from Titan's ionosphere, *Space Sci. Rev.*, *162*, 85–111, doi:10.1007/s11214-011-9826-4.

Coates, A. J., S. M. E. Tsang, A. Wellbrock, R. A. Frahm, J. D. Winningham, S. Barabash, R. Lundin, D. T. Young, and F. J. Crary (2011b), Ionospheric photoelectrons: Comparing Venus, Earth, Mars and Titan, *Planet. Space Sci.*, *59*, 1019–1027, doi:10.1016/j.pss.2010.07.016.

Cravens, T. E., R. V. Yelle, J.-E. Wahlund, D. E. Shemansky, and A. F. Nagy (2009), Composition and structure of the ionosphere and thermosphere, in *Titan From Cassini-Huygens*, edited by R. H. Brown, J.-P. Lebreton, and J. H. Waite, chap. 11, pp. 259–295, Springer, New York, doi:10.1007/978-1-4020-9215-2_11.

Edberg, N. J. T., K. Agren, J.-E. Wahlund, M. W. Morooka, D. J. Andrews, S. W. H. Cowley, A. Wellbrock, A. J. Coates, C. Bertucci, and M. K. Dougherty (2011), Structured ionospheric outflow during the Cassini Titan Flybys T55–T59, *Planet. Space Sci.*, *59*, 788–797, doi:10.1016/j.pss.2011.03.007.

Elrod, M. K., W.-L. Tseng, R. J. Wilson, and R. E. Johnson (2012), Seasonal variations in Saturn's plasma between the main rings and Enceladus, *J. Geophys. Res.*, *117*, A03207, doi:10.1029/2011JA017332.

Fedorov, A., S. Barabash, J. A. Sauvaud, Y. Futaana, T. L. Zhang, R. Lundin, and C. Ferrier (2011), Measurements of the ion escape rates from Venus for solar minimum, *J. Geophys. Res.*, *116*, A07220, doi:10.1029/2011JA016427.

Ganguli, S. B. (1996), The polar wind, *Rev. Geophys.*, *34*, 311–348, doi:10.1029/96RG00497.

Hartle, R. E., et al. (2006), Initial interpretation of Titan plasma interaction as observed by the Cassini plasma spectrometer: Comparisons with Voyager 1, *Planet. Space Sci.*, *54*, 1211–1224, doi:10.1016/j.pss.2006.05.029.

Johnson, R. E., O. J. Tucker, M. Michael, E. C. Sittler, H. T. Smith, D. T. Young, and J. H. Waite (2009), Mass loss processes in Titan's upper atmosphere, in *Titan From Cassini-Huygens*, edited by R. H. Brown, J.-P. Lebreton, and J. H. Waite, chap. 15, pp. 373–391, Springer, New York, doi:10.1007/978-1-4020-9215-2_15.

Kallio, E., I. Sillanpää, R. Jarvinen, P. Janhunen, M. Dougherty, C. Bertucci, and F. Neubauer (2007), Morphology of the magnetic field near Titan: Hybrid model study of the Cassini T9 flyby, *Geophys. Res. Lett.*, *34*, L24S09, doi:10.1029/2007GL030827.

Lewis, G. R., N. Andre, C. S. Arridge, A. J. Coates, L. K. Gilbert, D. R. Linder, and A. M. Rymer (2008), Derivation of density and temperature from the Cassini-Huygens CAPS electron spectrometer, *Planet. Space Sci.*, *56*, 901–912, doi:10.1016/j.pss.2007.12.017.

Lewis, G. R., et al. (2010), In-flight calibration of the Cassini-Huygens CAPS electron spectrometer, *Planet. Space Sci.*, *58*, 427–436, doi:10.1016/j.pss.2009.11.008.

Linder, D. R., A. J. Coates, R. D. Woodliffe, C. Alsop, A. D. Johnstone, M. Grande, A. Preece, B. Narheim, K. Svenes, and D. T. Young (1998), The Cassini CAPS electron spectrometer, in *Measurement Techniques in Space Plasmas: Particles*, *Geophys. Monogr. Ser*, vol. 102, edited by R. E. Pfaff, J. E. Borovsky, and D. T. Young, pp. 257–262, AGU, Washington, D. C., doi:10.1029/GM102p0257.

Lipatov, A. S., K. Sauer, and K. Baumgaertel (1997), 2.5D hybrid code simulation of the solar wind interaction with weak comets and related objects, *Adv. Space Res.*, *20*, 279–282, doi:10.1016/S0273-1177(97)00547-4.

Lipatov, A. S., E. C. Sittler Jr., R. E. Hartle, J. F. Cooper, and D. G. Simpson (2011), Background and pickup ion velocity distribution dynamics in Titan's plasma environment: 3D hybrid simulation and comparison with CAPS observations, *Adv. Space Res.*, *48*, 1114–1125, doi:10.1016/j.asr.2011.05.026.

Lipatov, A. S., E. C. Sittler Jr., R. E. Hartle, J. F. Cooper, and D. G. Simpson (2012), Saturn's magnetosphere interaction with Titan for T9 encounter: 3D hybrid modeling and comparison with CAPS observations, *Planet. Space Sci.*, *61*, 66–78, doi:10.1016/j.pss.2011.08.017.

Lundin, R. (2011), Ion acceleration and outflow from Mars and Venus: An overview, *Space Sci. Rev.*, *162*, 309–334, doi:10.1007/s11214-011-9811-y.

Ma, Y., A. F. Nagy, T. E. Cravens, I. V. Sokolov, K. C. Hansen, J.-E. Wahlund, F. J. Crary, A. J. Coates, and M. K. Dougherty (2006), Comparisons between MHD model calculations and observations of Cassini flybys of Titan, *J. Geophys. Res.*, *111*, A05207, doi:10.1029/2005JA011481.

Ma, Y.-J., et al. (2007), 3D global multi-species Hall-MHD simulation of the Cassini T9 flyby, *Geophys. Res. Lett.*, *34*, L24S10, doi:10.1029/2007GL031627.

Modolo, R., J.-E. Wahlund, R. Bostrom, P. Canu, W. S. Kurth, D. Gurnett, G. R. Lewis, and A. J. Coates (2007a), The far plasma wake of Titan from the RPWS observations: A case study, *Geophys. Res. Lett.*, *34*, L24S04, doi:10.1029/2007GL030482.

Modolo, R., G. M. Chanteur, J.-E. Wahlund, P. Canu, W. S. Kurth, D. Gurnett, A. P. Matthews, and C. Bertucci (2007b), Plasma environment in the wake of Titan from hybrid simulation: A case study, *Geophys. Res. Lett.*, *34*, L24S07, doi:10.1029/2007GL030489.

Nagy, A. F., Y. Liu, K. C. Hansen, K. Kabin, T. I. Gombosi, M. R. Combi, D. L. DeZeeuw, K. G. Powell, and A. J. Kliore (2001), The interaction between the magnetosphere of Saturn and Titan's ionosphere, *J. Geophys. Res.*, *106*, 6151–6160, doi:10.1029/2000JA000183.

Rymer, A. M., H. T. Smith, A. Wellbrock, A. J. Coates, and D. T. Young (2009), Discrete classification and electron energy spectra of Titan's varied magnetospheric environment, *Geophys. Res. Lett.*, *36*, L15109, doi:10.1029/2009GL039427.

Sillanpää, I., E. Kallio, P. Janhunen, W. Schmidt, K. Mursula, J. Vilppola, and P. Tanskanen (2006), Hybrid simulation study of ion escape at Titan for different orbital positions, *Adv. Space Res.*, *38*, 799–805, doi:10.1016/j.asr.2006.01.005.

Simon, S., G. Kleindienst, A. Boesswetter, T. Bagdonat, U. Motschmann, K.-H. Glassmeier, J. Schuele, C. Bertucci, and M. K. Dougherty (2007), Hybrid simulation of Titan's magnetic field signature during the Cassini T9 flyby, *Geophys. Res. Lett.*, *34*, L24S08, doi:10.1029/2007GL029967.

Simon, S., F. M. Neubauer, C. L. Bertucci, H. Kriegel, J. Saur, C. T. Russell, and M. K. Dougherty (2010), Titan's highly dynamic magnetic environment: A systematic survey of Cassini magnetometer observations from flybys TA–T62, *Planet. Space Sci.*, *58*(10), 1230–1251, doi:10.1016/j.pss.2010.04.021.

Sittler, E. C., Jr., R. E. Hartle, A. F. Viñas, R. E. Johnson, H. T. Smith, and I. Meuller-Wodarg (2005), Titan interaction with Saturn's magnetosphere: Voyager 1 results revisited, *J. Geophys. Res.*, *110*, A09302, doi:10.1029/2004JA010759.

Sittler, E. C., Jr., R. E. Hartle, C. Bertucci, A. Andrews, T. Cravens, I. Dandouras, and D. Shemansky (2009), Energy deposition processes in Titan's upper atmosphere and its induced magnetosphere, in *Titan From Cassini-Huygens*, edited by R. H. Brown, J.-P. Lebreton, and J. H. Waite, chap. 16, pp. 393–453, Springer, New York, doi:10.1007/978-1-4020-9215-2_16.

Sittler, E. C., Jr., et al. (2010), Saturn's magnetospheric interaction with Titan as defined by Cassini encounters T9 and T18: New results, *Planet. Space Sci.*, *58*, 327–350, doi:10.1016/j.pss.2009.09.017.

Smith, H. T. (2010), Neutral clouds and their influence on pick-up ions in Saturn's magnetosphere, in *Pickup Ions Throughout the Heliosphere and Beyond: Proceedings of the 9th Annual International Astrophysics Conference*, edited by J. le Roux et al., *AIP Conf. Proc.*, *1302*, 256–262.

Snowden, D., R. Winglee, and A. Kidder (2011), Titan at the edge: 1. Titan's interaction with Saturn's magnetosphere in the prenoon sector, *J. Geophys. Res.*, *116*, A08229, doi:10.1029/2011JA016435.

Szego, K., Z. Bebesi, C. Bertucci, A. J. Coates, F. Crary, G. Erdos, R. Hartle, E. C. Sittler, and D. T. Young (2007), The charged particle environment of Titan during the T9 flyby, *Geophys. Res. Lett.*, *34*, L24S03, doi:10.1029/2007GL030677.

Szego, K., Z. Nemeth, G. Erdos, L. Foldy, M. Thomsen, and D. Delapp (2011), The plasma environment of Titan: The magnetodisk of Saturn near the encounters as derived from ion densities measured by the Cassini/CAPS plasma spectrometer, *J. Geophys. Res.*, *116*, A10219, doi:10.1029/2011JA016629.

Thomsen, M. F., D. B. Reisenfeld, D. Delapp, R. L. Tokar, D. T. Young, F. J. Crary, E. C. Sittler, M. A. McGraw, and J. D. Williams (2010), Survey of ion plasma parameters in Saturn's magnetosphere, *J. Geophys. Res.*, *115*, A10220, doi:10.1029/2010JA015267.

Tseng, W.-L., W.-H. Ip, R. E. Johnson, T. A. Cassidy, and M. K. Elrod (2010), The structure and time variability of the ring atmosphere and ionosphere, *Icarus*, *206*(2), 382–389, doi:10.1016/j.icarus.2009.05.019.

Wahlund, J.-E., et al. (2005), Cassini measurements of cold plasma in the ionosphere of Titan, *Science*, *308*, 986–989, doi:10.1126/science.1109807.

Wei, H. Y., C. T. Russell, J.-E. Wahlund, M. K. Dougherty, C. Bertucci, R. Modolo, Y. J. Ma, and F. M. Neubauer (2007), Cold ionospheric plasma in Titan's magnetotail, *Geophys. Res. Lett.*, *34*, L24S06, doi:10.1029/2007GL030701.

Wei, H. Y., C. T. Russell, M. K. Dougherty, Y. J. Ma, K. C. Hansen, H. J. McAndrews, A. Wellbrock, A. J. Coates, M. F. Thomsen, and D. T. Young (2011), Unusually strong magnetic fields in Titan's ionosphere: T42 case study, *Adv. Space Res.*, *48*, 314–322, doi:10.1016/j.asr.2011.02.009.

Wellbrock, A., A. J. Coates, I. Sillanpää, G. H. Jones, C. S. Arridge, G. R. Lewis, D. T. Young, F. J. Crary, and A. D. Aylward (2012), Cassini observations of ionospheric photoelectrons at large distances from Titan: Implications for Titan's exospheric environment and magnetic tail, *J. Geophys. Res.*, *117*, A03216, doi:10.1029/2011JA017113.

Young, D. T., et al. (2004), Cassini plasma spectrometer investigation, *Space Sci. Rev.*, *114*, 1–112, doi:10.1007/s11214-004-1406-4.